AD-A148 016 THERMOSONDE C2N MEASUREMENTS IN HAWAII--AUGUST 1982(U) 1/1
AIR FORCE GEOPHYSICS LAB HANSCOM AFB MA
J H BROWN ET AL. 24 FEB 84 AFGL-TR-84-0110

UNCLASSIFIED F/G 4/2 NL

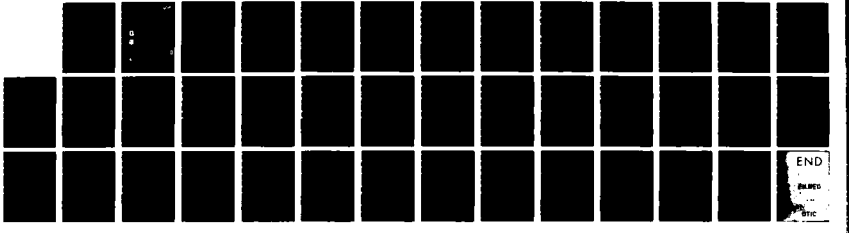

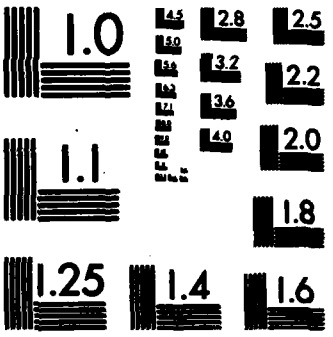

MICROCOPY RESOLUTION TEST CHART
NATIONAL BUREAU OF STANDARDS-1963-A

AFGL-TR-84-0110
ENVIRONMENTAL RESEARCH PAPERS, NO. 877

Thermosonde C_n^2 Measurements in Hawaii — August 1982

JAMES H. BROWN
ROBERT E. GOOD

24 February 1984

Approved for public release; distribution unlimited.

AD-A148 016

DTIC FILE COPY

DTIC
ELECTE
NOV 16 1984
S D
D

OPTICAL PHYSICS DIVISION PROJECT 7670
AIR FORCE GEOPHYSICS LABORATORY
HANSCOM AFB, MA 01731

84 11 05 079

This report has been reviewed by the ESD Public Affairs Office (PA) and is releasable to the National Technical Information Service (NTIS).

This technical report has been reviewed and is approved for publication.

FOR THE COMMANDER

ROBERT W. FENN
Branch Chief

JOHN S. GARING
Division Director

Qualified requestors may obtain additional copies from the Defense Technical Information Center. All others should apply to the National Technical Information Service.

If your address has changed, or if you wish to be removed from the mailing list, or if the addressee is no longer employed by your organization, please notify AFGL/DAA, Hanscom AFB, MA 01731. This will assist us in maintaining a current mailing list.

Do not return copies of this report unless contractual obligation or notices on a specific document requires that it be returned.

Unclassified

SECURITY CLASSIFICATION OF THIS PAGE

REPORT DOCUMENTATION PAGE

1a. REPORT SECURITY CLASSIFICATION Unclassified	1b. RESTRICTIVE MARKINGS
2a. SECURITY CLASSIFICATION AUTHORITY	3. DISTRIBUTION/AVAILABILITY OF REPORT Approved for public release; Distribution unlimited.
2b. DECLASSIFICATION/DOWNGRADING SCHEDULE	
4. PERFORMING ORGANIZATION REPORT NUMBER(S) AFGL-TR-84-0110 ERP, No. 877	5. MONITORING ORGANIZATION REPORT NUMBER(S)
6a. NAME OF PERFORMING ORGANIZATION Air Force Geophysics Laboratory 6b. OFFICE SYMBOL (If applicable) OPA	7a. NAME OF MONITORING ORGANIZATION
6c. ADDRESS (City, State and ZIP Code) Hanscom AFB Massachusetts 01731	7b. ADDRESS (City, State and ZIP Code)
8a. NAME OF FUNDING/SPONSORING ORGANIZATION 8b. OFFICE SYMBOL (If applicable)	9. PROCUREMENT INSTRUMENT IDENTIFICATION NUMBER
8c. ADDRESS (City, State and ZIP Code)	10. SOURCE OF FUNDING NOS. PROGRAM ELEMENT NO.: 62101F PROJECT NO.: 7670 TASK NO.: 15 WORK UNIT NO.: 07
11. TITLE (Include Security Classification) THERMOSONDE C_n^2 MEASUREMENTS IN HAWAII - (contd)	
12. PERSONAL AUTHOR(S) James H. Brown, Robert E. Good	
13a. TYPE OF REPORT Scientific Interim 13b. TIME COVERED FROM _____ TO _____	14. DATE OF REPORT (Yr., Mo., Day) 1984 February 24 15. PAGE COUNT 39
16. SUPPLEMENTARY NOTATION	
17. COSATI CODES FIELD / GROUP / SUB. GR.	18. SUBJECT TERMS (Continue on reverse if necessary and identify by block number) Optical turbulence, Turbulence, C_n^2, Refractive structure, Coherence, Isoplanatism, Radiosonde, Thermosonde, Scintillation

19. ABSTRACT (Continue on reverse if necessary and identify by block number)

C sub n squared

→ Eight AFGL thermosondes were flown from Mt. Haleakala, Hawaii to measure atmospheric turbulence in the form of the optical refractive index structure constant (C_n^2). Temperature and relative humidity comparisons between the AFGL instruments and standard GMD rawinsondes are presented. The AFGL instruments obtain greater temperature and humidity spatial resolution and consequently show finer structure in the profiles. A diurnal shift in the (C_n^2) profile is noted as well as a tropopause enhancement. Coherence scales are calculated from the thermosonde data.

C sub-n squared

20. DISTRIBUTION/AVAILABILITY OF ABSTRACT UNCLASSIFIED/UNLIMITED ☒ SAME AS RPT. ☐ OTIC USERS ☐	21. ABSTRACT SECURITY CLASSIFICATION Unclassified
22a. NAME OF RESPONSIBLE INDIVIDUAL James H. Brown	22b. TELEPHONE NUMBER (Include Area Code) x5779 22c. OFFICE SYMBOL OPA

DD FORM 1473, 83 APR EDITION OF 1 JAN 73 IS OBSOLETE.

Unclassified

SECURITY CLASSIFICATION OF THIS PAGE

Block 11 (contd)

AUGUST 1982

Accession For	
NTIS GRA&I	X
DTIC TAB	☐
Unannounced	☐
Justification	
By	
Distribution/	
Availability Codes	
Dist	Avail and/or Special
A/1	

Preface

The following individuals participated in data gathering and reduction:

Telemetry	Mr. J. Griffin, LCR
Data Reduction	Ms. P. Bench, LKD Ms. D. Pelekasis, RMA Dr. B. Beland, Rio Grande Assoc. Mr. B. Bletsis, Rio Grande Assoc.
GMD radiosondes	5th Weather Squadron, AWS

Contents

1. INTRODUCTION 9

2. THERMOSONDE DESCRIPTION 10

3. FLIGHT RESULTS 10

4. DATA ANALYSIS 12
   - 4.1 C_n^2 Profiles 12
   - 4.2 Temperature and Humidity Comparison 13
   - 4.3 Average Profile 15
   - 4.4 Coherence Scales 16
   - 4.5 Examination of possible Measurement Contamination due to Balloon Wake 18

REFERENCES 39

Illustrations

1. Comparison Between Ambient Temperature Profile as Measured by Thermosonde 2X0012 and as Measured by Standard GMD Radiosonde, Ascent 8. Launched 13 Aug 1982, 1041Z 20

2. Comparison Between Ambient Temperature Profile as Measured by Thermosonde 2X0001 and as Measured by Standard GMD Radiosonde, Ascent 12. Launched 20 Aug 1982, 0804Z 20

3. Comparison Between Ambient Temperature Profile as Measured by Thermosonde 2X0005 and as Measured by Standard GMD Radiosonde, Ascent 12. Launched 20 Aug 1982, 1001Z 21

4. Comparison Between Ambient Temperature Profile as Measured by Thermosonde 2X0038 and as Measured by Standard GMD Radiosonde, Ascent 15. Launched 21 Aug 1982, 0654Z 21

5. Comparison Between Ambient Temperature Profile as Measured by Thermosonde 2X0045 and as Measured by Standard GMD Radiosonde, Ascent 16. Launched 21 Aug 1982, 0826Z 22

6. Comparison Between Ambient Temperature Profile as Measured by Thermosonde 2X0037 and as Measured by Standard GMD Radiosonde, Ascent 19. Launched 22 Aug 1982, 0709Z 22

7. Comparison Between Ambient Temperature Profile as Measured by Thermosonde 2X0049 and as Measured by Standard GMD Radiosonde, Ascent 19. Launched 22 Aug 1982, 0905Z 23

8. Comparison Between Ambient Temperature Profile as Measured by Thermosonde 2X0022 and as Measured by Standard GMD Radiosonde, Ascent 21. Launched 24 Aug 1982, 0909Z 23

9. Comparison Between Relative Humidity Profile as Measured by Thermosonde 2X0012 and as Measured by Standard GMD Radiosonde, Ascent 8. Launched 13 Aug 1982, 1041Z 24

10. Comparison Between Relative Humidity Profile as Measured by Thermosonde 2X0001 and as Measured by Standard GMD Radiosonde, Ascent 12. Launched 20 Aug 1982, 0804Z 24

11. Comparison Between Relative Humidity Profile as Measured by Thermosonde 2X0005 and as Measured by Standard GMD Radiosonde, Ascent 12. Launched 20 Aug 1982, 1001Z 25

12. Comparison Between Relative Humidity Profile as Measured by Thermosonde 2X0038 and as Measured by Standard GMD Radiosonde, Ascent 15. Launched 21 Aug 1982, 0654Z 25

13. Comparison Between Relative Humidity Profile as Measured by Thermosonde 2X0045 and as Measured by Standard GMD Radiosonde, Ascent 16. Launched 21 Aug 1982, 0826Z 26

14. Comparison Between Relative Humidity Profile as Measured by Thermosonde 2X0037 and as Measured by Standard GMD Radiosonde, Ascent 19. Launched 22 Aug 1982, 0709Z 26

15. Comparison Between Relative Humidity Profile as Measured by Thermosonde 2X0049 and as Measured by Standard GMD Radiosonde, Ascent 19. Launched 22 Aug 1982, 0905Z 27

16. Comparison Between Relative Humidity Profile as Measured by Thermosonde 2X0022 and as Measured by Standard GMD Radiosonde, Ascent 21. Launched 24 Aug 1982, 0909Z 27

17. Comparison Between Wind Profile as Measured by Thermosonde 2X0012 and Standard GMD Radiosonde, Ascent 8. Launched 13 Aug 1982, 1041Z 28

18. Comparison Between Wind Profile as Measured by Thermosonde 2X0001 and Standard GMD Radiosonde, Ascent 12. Launched 20 Aug 1982, 0804Z 28

19. Comparison Between Wind Profile as Measured by Thermosonde 2X0005 and Standard GMD Radiosonde, Ascent 12. Launched 20 Aug 1982, 1001Z 29

20. Comparison Between Wind Profile as Measured by Thermosonde 2X0038 and Standard GMD Radiosonde, Ascent 15. Launched 21 Aug 1982, 0654Z 29

21. Comparison Between Wind Profile as Measured by Thermosonde 2X0045 and Standard GMD Radiosonde, Ascent 16. Launched 21 Aug 1982, 0826Z 30

22. Comparison Between Wind Profile as Measured by Thermosonde 2X0037 and Standard GMD Radiosonde, Ascent 19. Launched 22 Aug 1982, 0709Z 30

23. Comparison Between Wind Profile as Measured by Thermosonde 2X0049 and Standard GMD Radiosonde, Ascent 19. Launched 22 Aug 1982, 0905Z 31

24. Comparison Between Wind Profile as Measured by Thermosonde 2X0022 and Standard GMD Radiosonde, Ascent 21. Launched 24 Aug 1982, 0909Z 31

25. Comparison of 500-m Log-Averaged Thermosonde C_n^2 Profile (Mean Bracketed by Mean Multiplied by 1 Sigma and Mean Divided by 1 Sigma) and Hufnagel Model (Thick Line) for Thermosonde 2X0012 and Standard GMD Radiosonde, Ascent 8. Launched 13 Aug 1982, 1041Z 32

26. Comparison of 500-m Log-Averaged Thermosonde C_n^2 Profile (Mean Bracketed by Mean Multiplied by 1 Sigma and Mean Divided by 1 Sigma) and Hufnagel Model (Thick Line) for Thermosonde 2X0001 and Standard GMD Radiosonde, Ascent 12. Launched 20 Aug 1982, 0804Z 32

27. Comparison of 500-m Log-Averaged Thermosonde C_n^2 Profile (Mean Bracketed by Mean Multiplied by 1 Sigma and Mean Divided by 1 Sigma) and Hufnagel Model (Thick Line) for Thermosonde 2X0005 and Standard GMD Radiosonde, Ascent 12. Launched 20 Aug 1982, 1001Z 33

28. Comparison of 500-m Log-Averaged Thermosonde C_n^2 Profile (Mean Bracketed by Mean Multiplied by 1 Sigma and Mean Divided by 1 Sigma) and Hufnagel Model (Thick Line) for Thermosonde 2X0038 and Standard GMD Radiosonde, Ascent 15. Launched 21 Aug 1982, 0654Z 33

29. Comparison of 500-m Log-Averaged Thermosonde C_n^2 Profile (Mean Bracketed by Mean Multiplied by 1 Sigma and Mean Divided by 1 Sigma) and Hufnagel Model (Thick Line) for Thermosonde 2X0045 and Standard GMD Radiosonde, Ascent 16. Launched 21 Aug 1982, 0826Z 34

30. Comparison of 500-m Log-Averaged Thermosonde C_n^2 Profile (Mean Bracketed by Mean Multiplied by 1 Sigma and Mean Divided by 1 Sigma) and Hufnagel Model (Thick Line) for Thermosonde 2X0037 and Standard GMD Radiosonde, Ascent 19. Launched 22 Aug 1982, 0709Z 34

31. Comparison of 500-m Log-Averaged Thermosonde C_n^2 Profile (Mean Bracketed by Mean Multiplied by 1 Sigma and Mean Divided by 1 Sigma) and Hufnagel Model (Thick Line) for Thermosonde 2X0049 and Standard GMD Radiosonde, Ascent 19. Launched 22 Aug 1982, 0905Z 35

32. Comparison of 500-m Log-Averaged Thermosonde C_n^2 Profile (Mean Bracketed by Mean Multiplied by 1 Sigma and Mean Divided by 1 Sigma) and Hufnagel Model (Thick Line) for Thermosonde 2X0022 and Standard GMD Radiosonde, Ascent 21. Launched 24 Aug 1982, 0909Z 35

33. Comparison of Log-Averaged Thermosonde C_n^2 for Eight Flights and AMOS Model 36

34. Comparison of PSDs for 18 m, 37 m, and 55 m Suspension Lengths, at Sample Altitude 37

35. Comparison of PSDs for 18 m, 37 m, and 55 m Suspension Lengths, Averaged Over the Entire Altitude Region 37

Tables

1. Schedule of Launches, Train Lengths, Maximum Altitudes, and Mean Square Wind Speeds 11

2. Temperature and Humidity Statistics 14

3. Coherence Scales 17

Thermosonde C_n^2 Measurements in Hawaii - August 1982

1. INTRODUCTION

Eight AFGL thermosondes [1] were flown from Mt. Haleakala, Maui, Hawaii during August 1982. The purpose was to measure upper air pressure, temperature, relative humidity, winds, and temperature fluctuations to quantify the atmospheric optical structure constant, C_n^2. Fluctuations of the refractive index, characterized as C_n^2, are important in determining how an electromagnetic wave will be disturbed along its propagation path in a turbulent environment.[2] Turbulence causes amplitude fluctuations of light (for example, stars twinkle) and phase distortions of a coherent laser beam. C_n^2 measurements and model predictions are needed for determining optical instrument design criteria and effects upon the control systems of compensated imaging devices.

These experiments were conducted at the ARPA Maui Optical Station (AMOS)

(Received for publication 22 Feb 1984)

1. Brown, J.H., Good, R.E., Bench, P.M., and Faucher, G.E. (1982) Sonde Experiments for Comparative Measurements of Optical Turbulence, AFGL-TR-82-0079, AD A118740.
2. Good, R.E., Brown, J.H., and Quesada, A.F. (1982) Measurements of high altitude resolution C_n^2 profiles and their importance on coherence lengths, SPIE Proc., 365:105-111.

in conjunction with the Advanced Multicolor Tracker for AMOS (AMTA) calibration and atmospheric transmission (A-CAT) experiment.[3]

2. THERMOSONDE DESCRIPTION

The Thermosonde system is comprised of a VIZ modified "artsonde" and AFGL micro-thermal bridge.[1] Pressure, temperature, and humidity data are measured every 2 sec by the artsonde as the balloon ascends from ground level to about 30 km. Concurrently, RMS temperature fluctuations, C_T, are measured by the thermosonde bridge circuit and these are transmitted on spare artsonde channels. C_n^2 is calculated from:

$$C_n^2(z) = \left[\frac{79.9 \times 10^{-6} P(z)}{T_K^2(z)}\right]^2 C_T^2(z) \qquad (1)$$

where P(z) is the pressure in mbar, $T_K(z)$ is the Kelvin temperature, and z is altitude.

Two unheated fine wire tungsten probes, separated 1 m horizontally form two arms of an AC Wheatstone bridge. A suppressed carrier modulation technique is used to detect and amplify small resistance changes across the bridge. The signal is further amplified, band pass filtered, and averaged in a 1-sec root-mean-square module. The voltage output is then converted to an electrical current that drives the artsonde oscillator.

To calibrate the device, the radiosonde frequency is correlated with known resistance imbalances across the bridge. The calibration temperature imbalance is then a simple function of the probe temperature coefficient[1].

3. FLIGHT RESULTS

Eight payloads were balloon-launched on five nights in August 1982 from near the top of Mt. Haleakala. Unusual weather-front disturbances caused cancellation on ten nights. Low and high clouds, high humidities and high winds contributed to several aborted launch attempts.

To avoid turbulent shedding effects from the 2-m balloon, the payload is automatically reeled down immediately after launch. Train lengths ranging from 18 m

---

3. Chapman, J.C. (1981) Groundbased infrared measurements using the AMOS/MOTIF facility, SPIE Proc., 280:186-193.

to 79 m were used to determine if wake effects were present in the thermosonde measurements.

Standard radiosondes were launched before and after the thermosondes. Since the standard radiosondes report only mandatory and significant levels, temperature and humidity comparisons with the thermosondes were desired to determine if significant structures were undetected by the standard radiosonde. A summary of the flights is shown in Table 1.

Table 1. Schedule of Launches, Train Lengths, Maximum Altitudes, and Mean Square Wind Speeds

Thermosonde						STD Radiosonde		
LAUNCH		ID	TRAIN LENGTH	MAX ALT	$\overline{W^2}$	LAUNCH		ΔTIME
Date(Z)	Time(Z)		(m)	(km)	$(m/sec)^2$	Time(Z)	ACST#	(hr, min)
13 Aug	104104	2X0012	79.	28.	197.	124300	8	$-2^h\ 02^m$
20 Aug	080400	2X0001	37.	27.	198.	055100	12	$+2^h\ 13^m$
20 Aug	100051	2X0005	55.	27.	198.	055100	12	$+4^h\ 10^m$
21 Aug	065412	2X0038	37.	18.	235.	045800	15	$+1^h\ 56^m$
21 Aug	082616	2X0045	18.	13.	329.	101000	16	$-1^h\ 44^m$
22 Aug	070909	2X0037	37.	19.	503.	050000	19	$+2^h\ 09^m$
22 Aug	090447	2X0049	18.	24.	503.	050000	19	$+4^h\ 05^m$
24 Aug	090844	2X0022	37.	13.	110.	192600	21	$-10^h\ 17^m$

MAX ALT = maximum altitude for which data are recorded.
$\overline{W^2}$ = mean square wind speed, 5 km to 20 km (or max alt).
ΔTIME = time of thermosonde launch relative to closest standard radiosonde flight.

Altitude profiles of temperature, relative humidity, winds-aloft and smoothed C_n^2 are presented in Figures 1-32. These figures will be explained below. The standard radiosonde temperature and relative humidity points have been plotted on the same graph as the thermosonde temperature and relative humidity, where appropriate, for visual comparison. Clearly, the standard measurements smooth much of the data. The mean square wind speed for each wind profile is

calculated to estimate a C_n^2 profile from the Hufnagel model.[4] These model profiles are drawn in as a dark line on the smoothed thermosonde C_n^2 graphs. Also shown on the smoothed C_n^2 plots are curves representing C_n^2 multiplied by and divided by 1 standard deviation of the mean.

4. DATA ANALYSIS

4.1 C_n^2 Profiles

To smooth the raw C_n^2 data, 500-m weighted log averages were taken. Weighting compensates for noise limited data. The noise limit is reached when regions of very low turbulence are encountered. The noise limit on the thermosonde is $C_T \leq 0.002°C$; hence, these values are not included in the log average since it is impossible to know the true low value of C_n^2. A conservative estimate of the average C_n^2 is obtained by weighting the values of C_n^2 measured above the noise level. However, the ratio of the number of signal points to the total number of points is used to multiply the log average as a weighting function. Thus,

$$C_n^2(z) = \frac{n}{N} \log^{-1}\left[\frac{1}{N}\sum_{i=1}^{n} \log C_{n_i}^2\right] \tag{2}$$

where, N is the total number of points over ΔZ = 500 m, and n is the total number minus the number of points in the noise. A log average of the data was performed since the raw data is represented by a log-normal distribution. Figures 25-32 (center curves) show the thermosonde log-average profiles for the eight flights. Shown on either side of the log-average curve is the mean multiplied by and divided by 1 standard deviation of the mean statistic. The curves are broken at those altitudes where telemetry was intermittent and the number of data points was small. Drawn between the broken curves are circles and squares depicting valid log-average data points and their standard deviation respectively. For the first 500 m above the surface, the actual instantaneous (not log-averaged) C_n^2 data are plotted. Since C_n^2 falls off extremely rapidly in the boundary layer, a 500 m log-average is not representative of the data in this region. Thus we have a composite curve showing the point measurement boundary layer turbulence as well as the upper altitude 500 m turbulent layering structure. These profiles are not to be

---

4. Hufnagel, R.E. (1974) Variations of Atmospheric Turbulence, The Infrared Handbook, USGPO, Washington, D.C., Chap. 6, pp. 1-56.

considered "snapshots" of $C_n^2(z)$ since the measurements are space- and time-dependent. However, the trend curve is considered valid over the length of the experiment and the turbulent structure is representative of a characteristic state.

Over-plotted on the C_n^2 profiles (Figures 25-32) are the mean-square wind speed dependent model curves. These are depicted by the solid dark line. These Hufnagel profiles[4] are for z = 6 km to 24 km constructed from the model.

$$C_n^2 \text{ (model)} = 2.7 \times 10^{-16} \left[3 \overline{W^2} \, e^{-z} \left(\frac{z}{10}\right)^{10} + e^{\left(\frac{-z}{1.5}\right)} \right]$$

where $\overline{W^2}$ is the mean square wind speed from 5 km to 20 km. The latter values are listed in Table 1 and are calculated for those flights only where sufficient wind data exists. The usual thermosonde/rawinsonde package measures winds-aloft at 1-sec intervals that are usually reduced to 30-sec averages. However, the usual telemetry equipment was not available for these flights. Instead, an Air Force GMD tracker was utilized to track the balloon. Thus, the resolution of the wind speed and direction (Figures 17-24) profiles is quite coarse. In any case, this is the resolution ordinarily used in the Hufnagel model.[4]

The comparison of thermosonde data with the Hufnagel model shows reasonable agreement at heights above the tropopause. However, below the tropopause, the Hufnagel model overestimated the C_n^2 by factors between 2 and 10. The reverse is true for one flight, 2X0012. Using the Hufnagel model to calculate the isoplanatic angle will yield an overestimate. Since the Hufnagel model is empirical and depends only on mean square wind speed, it would be useful to compare the thermosonde data with a VanZandt[5] model which depends on the Richardson number. This is being done in further studies.

4.2 Temperature and Humidity Comparison

The AFGL thermosondes report temperature and humidity measurements every 2 sec or almost every 10 m, whereas standard radiosonde data are tabulated only at significant levels. Figures 1-16 depict AFGL measurements by solid lines and standard sonde measurements as asterisks connected by straight lines. The much finer resolution of the AFGL measurements is clearly evident. The temperature comparisons show good agreement; however, the standard sonde provides

---

5. VanZandt, T.E., Gage, K.S., and Warnock, J.M. (1981) An improved model for the calculation of profiles of C_n^2 and ϵ in the free atmosphere from background profiles of wind, temperature and humidity, preprints 20th Conf. Radar Meteorol. Soc., Boston, Am. Meteorol. Soc., pp. 129-135.

only the trend line in humidity. The question we wish to answer is: does the coarseness of the standard humidity measurement cause significant errors in the calculation of the total water vapor content?

The difference in temperature and relative humidity between thermosonde and standard radiosonde can be represented as a mean deviation. We define the mean deviation as

$$\overline{\Delta T} = \frac{1}{N} \sum_{i=1}^{N} (T_T - T_R) ,$$

where T_T is temperature measured by the thermosonde and T_R is temperature measured by the standard radiosonde. A mean deviation will show a "bias" between the two sets of measurements. These differences are shown in Table 2.

Table 2. Temperature and Humidity Statistics

Flight #	Ascent #	n_t	n_u	$\overline{\Delta T}$ °C	$\overline{\Delta U}$ %	W_{ther} g.cm^{-2}	W_{AST} g.cm^{-2}
2X0012	8	20	12	0.2	-3.4	0.55	0.46
2X0001	12	41	23	-0.5	-2.0	1.24	1.20
2X0005	12	30	20	-0.1	-5.0	1.17	1.20
2X0038	15	37	27	0.9	1.9	0.97	1.10
2X0045	16	27	17	0.4	1.4	0.96	1.04
2X0037	19	25	18	0.3	-3.5	1.38	1.16
2X0049	19	33	18	0.4	-1.2	1.33	1.16
2X0022	21	14	10	0.5	-2.0	0.47	0.47

Flight# = Thermosonde flight identification number.

Ascent# = Standard rawinsonde identification number.

n_t = Number of temperature reports for standard sonde.

n_u = Number of relative humidity reports for standard sonde.

ΔT = Mean difference between temperature reported by thermosonde and standard sonde.

$\overline{\Delta U}$ = Mean difference between relative humidity reported by thermosonde and standard sonde.

W_{ther} = Water vapor column density as measured from thermosonde data.

W_{AST} = Water vapor column density as measured from standard sonde data.

Here n_t and n_u are the number of temperature and humidity points compared respectively. From inspection of the table, no real bias can be inferred between the two data sets.

As evident in Table 2, the relative humidity difference causes mild differences in the total water vapor content, W, with the maximum difference being about 16 percent. This difference is attributed to the large time differences between launches of the thermosonde and standard radiosonde. A second obervation is that although the temperature difference is small, minor tropospheric temperature inversions may not appear in the standard sonde data. This is evident in Figures 2 and 7, where the boundary layer inversion is hidden. Since several C_n^2 models depend on the height of the first inversion layer, this defect in the standard sonde resolution may very well be significant. Additionally, the AFGL thermosonde plots show fine structure in the stratospheric temperature profiles (Figures 1, 2, 3, and 7). This structure apparently represents coarse turbulence layering. To test whether the layering is real, a balloon may be used to carry two thermosondes, one below the other. The lower thermosonde should "see" the layer with an appropriate phase shift. Tests of this kind are presently being carried out. Where fine resolution radiosondes are available, this structure would be useful for refined C_n^2 models.

4.3 Average Profile

A log-average of 8 thermosonde C_n^2 profiles resulted in the average profile shown in Figure 33. For comparison, the AMOS model[6] is also plotted in Figure 33 as a solid dark line. Significant departure from the AMOS model is evident above 19 km and below 8 km. Also, the thermosonde data show a significant enhancement of C_n^2 near the tropopause. The total log-average thermosonde data were fit to an exponential model with an added Gaussian factor to account for the bulge at the tropopause.

The model is of the form:

$$\text{Log } C_n^2 = A + Bz + Cz^2 + D \exp\left[-\frac{1}{2}\left(\frac{z-E}{F}\right)^2\right]$$

---

6. Miller, M. G., and Zieske, P. L. (1979) Turbulence Environment Characterization, RADC-TR-79-131, AD A072379.

For $z > 5$ km, the fitted constants are:

	8-flights averaged
A	-17.417
B	0.0092
C	-0.0026
D	0.8094
E	14.855
F	1.523

The model suggests a maximum enhancement of C_n^2 at 14.7 km with a standard deviation of 1.5 km. For summer nighttime conditions, at the experiment coordinates, the model further suggests dropoff rates of 0.27 dB/km and 1.47 dB/km at 7 km and 30 km respectively.

4.4 Coherence Scales

For each flight, the transverse coherence length r_o and isoplanatic angle θ_o were calculated. The coherence length is calculated from the expression

$$r_o = 2.1 \quad [1.46\, k^2 \int_{z_o}^{z_f} C_n^2(z)\, dz]^{-3/5} \quad \text{(m)}$$

and the isoplanatic angle is calculated from the expression

$$\theta_o = [2.95\, k^2 \int_{z_o}^{z_f} C_n^2(z) z^{5/3}\, dz]^{-3/5} \quad \text{(rad)}$$

where the wave number k is $2\pi/\lambda$, z_o is observer altitude, and z_f is the maximum altitude. The coherence scales are distance and angular limits for which a wave front propagating through a turbulent atmosphere is coherent. In particular, isoplanatism denotes a region in the field of view over which the transfer function of an optical system is virtually independent of field angle. The practical meaning of isoplanatism is that it denotes the largest size field of view for which a particular system will work unaffected by the presence of atmospheric turbulence. It is significant in compensated imaging systems. The transverse coherence length denotes the largest beam diameter over which the beam is coherent. In particu-

lar, it specifies the limiting size of a telescope aperture for which turbulence phase front distortions are important.

Results of the above calculations are tabulated in Table 3. Here the non-

Table 3. Coherence Scales

Flight ID	Coherence Length, r_o(cm)	Isoplanatic angle, θ_o (μrad)	Hufnagel Model θ_o(μrad)
2X0012	3.8	2.0*	13.1
2X0001	6.3	12.8	9.94
2X0005	10.7	12.7	9.94
2X0038	12.5	7.5	9.2
2X0045	9.9	+	7.8
2X0037	7.3	3.8*	6.3
2X0049	8.4	6.5	6.3
2X0022	7.7	11.7+	7.01

* based on interpolation from only a few points near the tropopause.
+ no data above 13 km.

smoothed C_n^2 data were interpolated every 10 m, and when C_T was noise limited, C_n^2 was calculated from C_T (noise) = 0.002°. Gaps in the data are replaced by log-interpolated values. The observed C_n^2 profiles indicate that r_o has very little dependence on C_n^2 above several kilometers, and θ_o has little dependence on C_n^2 above 18 km. Flight 2X0045 was terminated prematurely at 13 km and consequently the isoplanatic angle cannot be computed. Flights 2X0012 and 2X0037 had large gaps in the observed data because the launch building blocked the tracking and reception of telemetry. Consequently, the calculation of isoplanatic angle based on interpolation can be in error. It is expected that the reported coherence scales err slightly on the high side because the noise level C_n^2 measurements were assumed where the actual C_n^2 could be less than the noise level.

The average coherence length for the flights is:

$$\overline{r_o} = 8.3 \pm 0.9\,\text{cm}$$

where the error is 1 standard deviation of the mean. Miller and Zieske[7] measured the coherence length from the same location and observed $5.3\,\text{cm} < \overline{r_o} < 17.8\,\text{cm}$. Their average for 24 nights conducted over a period of 8 months was $\overline{r_o} = 9.6\,\text{cm}$ with $\sigma = 2.2\,\text{cm}$. The small sample reported here is consistent with the previous data. The average isoplanatic angle for the five flights with valid data through the tropopause is:

$$\overline{\theta_o} = 10.2 \pm 1.3\ \mu\text{rad}$$

4.5 Examination of Possible Measurement Contamination due to Balloon Wake

The measurement of C_T with a thermosonde suspended below a rising balloon raises the question of whether balloon wakes cause any errors. At launch, the balloon has a diameter of about 2 m which expands to nearly 10 m at 30 km. There are several possible mechanisms for the balloon wake to introduce an erroneous C_T measurement. The balloon might cause a vertical mixing of the atmosphere over the balloon scale size. The thermosonde could then measure a temperature difference equal to that in the atmosphere over the height of the balloon. Another mechanism is for the wake to homogenize and dissipate by diffusion any pre-existing temperature differences in the atmosphere. A third possibility assumes that the balloon, because of different radiation absorption, is at a different temperature from the atmosphere. Consequently, the wake is a mixture of the atmospheric and balloon skin temperature. In summary, there are conceivable physical processes that can either enhance C_T or remove C_T.

One way of searching for balloon wake effect is to assume that the thermosonde suspended below the balloon acts as a pendulum. The thermosonde might then swing in and out of the wake. A frequency analysis of the C_T data could be used to identify any pronounced peaks or valleys to be associated with a wake effect. Thus, thermosondes were launched with different lengths between the balloon and the thermosonde. Flights with suspension lengths of 18 m, 37 m, and 55 m were used and pendulum frequencies 0.12 Hz, 0.08 Hz, and 0.07 Hz were examined in power spectral density plots of C_T. Figure 34 contains the power spec-

---

7. Miller, M. G., and Zieske, P. L. (1977) Measurement of the atmospheric correlation scale, J. Opt. Soc. Am., 67:1680-1685.

tral density, C_T^2/Hz for three different suspension lengths. A sample consisting of 128 consecutive data points taken at 2-sec intervals was used to perform the frequency analysis. The plots are displaced vertically for easier inspection on an arbitrary scale. It is apparent that there are no noticeable pendulum frequencies and no apparent systematic difference between the spectra of different lengths. It must be remembered that the data are obtained during ascent, and the sampling period represents data collected over a 1 km altitude region wherein lie the thin layers of turbulence.

Figure 35 contains the power spectral density of the same flights averaged over the entire altitude region. The PSD of approximately 20 spectra are linearly averaged. The flights are superimposed on an absolute scale. Again, there is no noticeable difference in the spectra, indicating that the length of the thermosonde suspension has no impact on the measurements. Of course, this assumes that there is a significant amount of payload swing at frequencies where the effect would show up. We have, therefore, assumed that there are no observable wake effects and that the thermosonde is measuring the actual turbulence temperature structure constants. That this is correct is supported by the comparison between radar and scintillometer measurements in conjunction with short train thermosonde[1,2,8] measurements.

---

8. Good, R.E., Watkins, B.J., Quesada, A.F., Brown, J.H., and Loriot, G.B. (1982) Radar and optical measurements of C_n^2, Appl. Opt., 21 (No. 18):3373-3376.

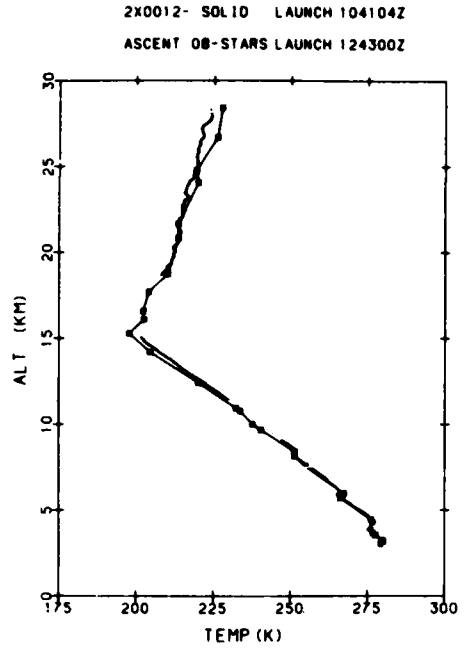

Figure 1. Comparison Between Ambient Temperature Profile as Measured by Thermosonde 2X0012 and as Measured by Standard GMD Radiosonde, Ascent 8, Launched 13 Aug 1982, 1041Z

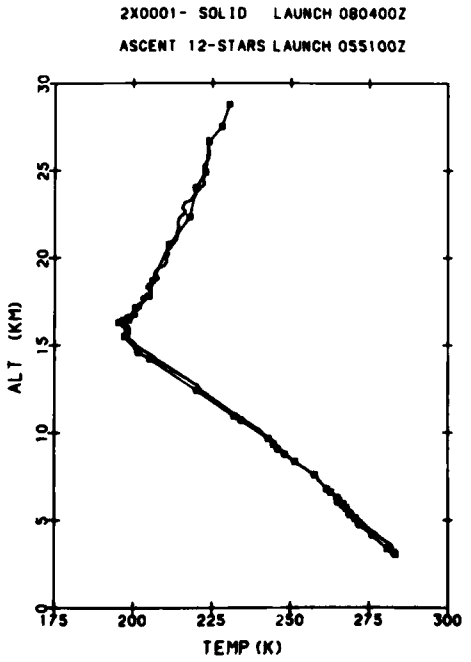

Figure 2. Comparison Between Ambient Temperature Profile as Measured by Thermosonde 2X0001 and as Measured by Standard GMD Radiosonde, Ascent 12. Launched 20 Aug 1982, 0804Z

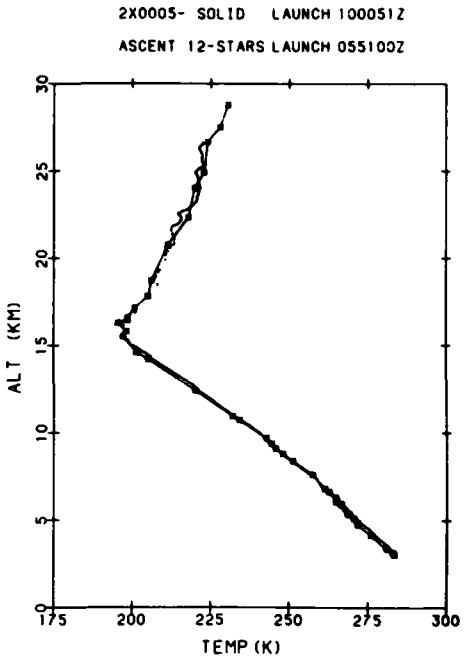

Figure 3. Comparison Between Ambient Temperature Profile as Measured by Thermosonde 2X0005 and as Measured by Standard GMD Radiosonde, Ascent 12. Launched 20 Aug 1982, 1001Z

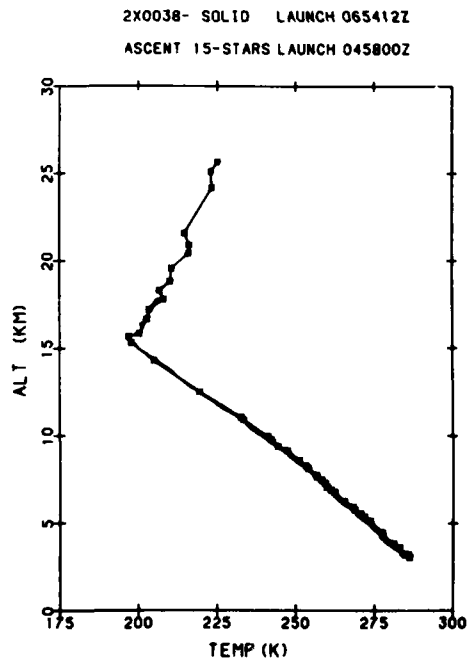

Figure 4. Comparison Between Ambient Temperature Profile as Measured by Thermosonde 2X0038 and as Measured by Standard GMD Radiosonde, Ascent 15. Launched 21 Aug 1982, 0654Z

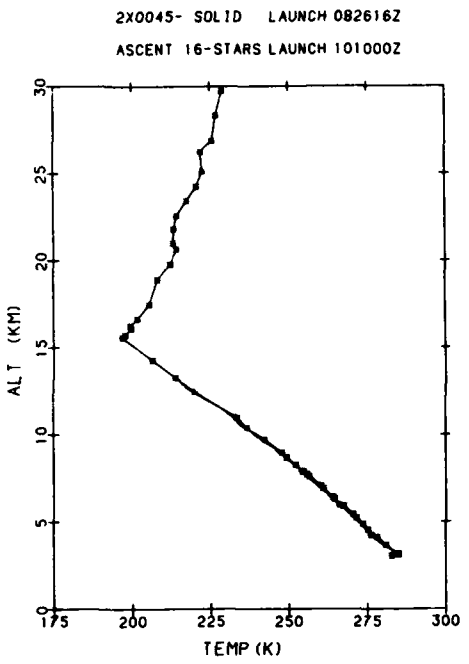

Figure 5. Comparison Between Ambient Temperature Profile as Measured by Thermosonde 2X0045 and as Measured by Standard GMD Radiosonde, Ascent 16. Launched 21 Aug 1982, 0826Z

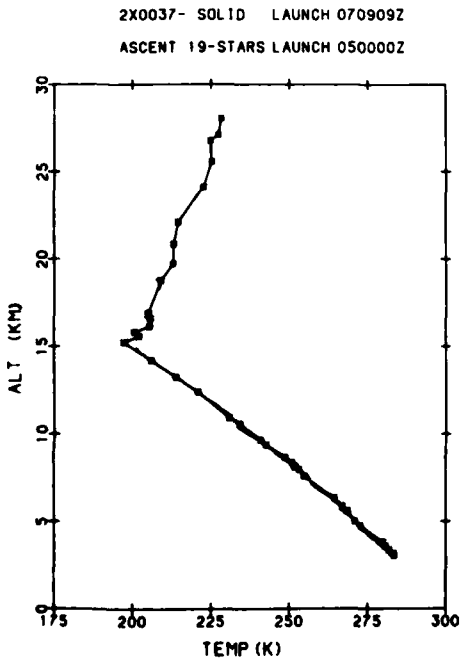

Figure 6. Comparison Between Ambient Temperature Profile as Measured by Thermosonde 2X0037 and as Measured by Standard GMD Radiosonde, Ascent 19. Launched 22 Aug 1982, 0709Z

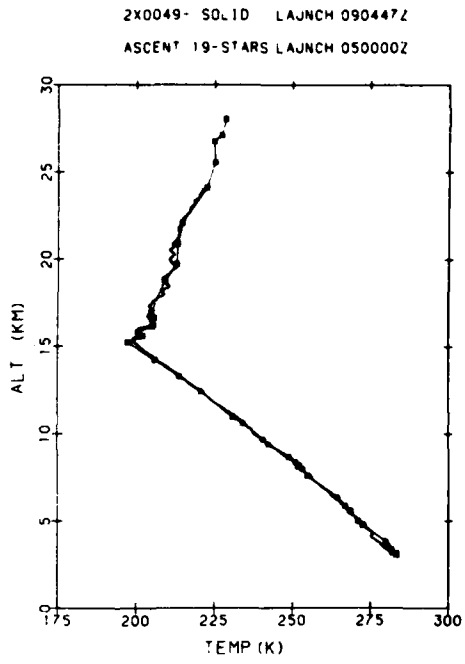

Figure 7. Comparison Between Ambient Temperature Profile as Measured by Thermosonde 2X0049 and as Measured by Standard GMD Radiosonde, Ascent 19. Launched 22 Aug 1982, 0905Z

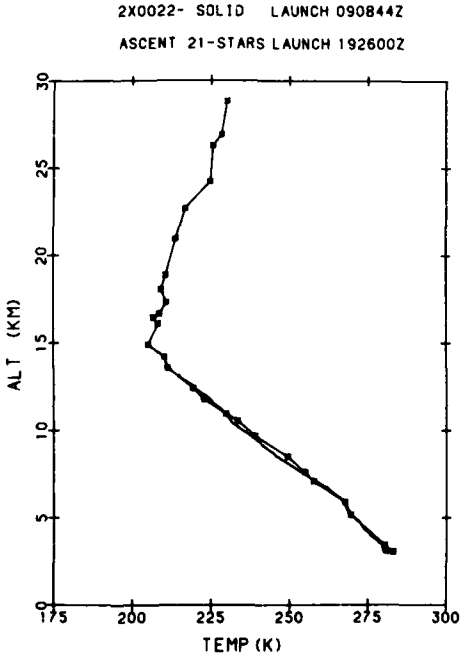

Figure 8. Comparison Between Ambient Temperature Profile as Measured by Thermosonde 2X0022 and as Measured by Standard GMD Radiosonde, Ascent 21. Launched 24 Aug 1982, 0909Z

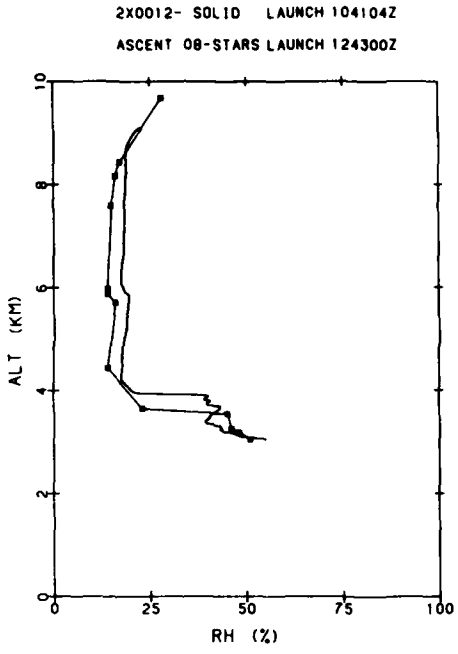

Figure 9. Comparison Between Relative Humidity Profile as Measured by Thermosonde 2X0012 and as Measured by Standard GMD Radiosonde, Ascent 8. Launched 13 Aug 1982, 1041Z

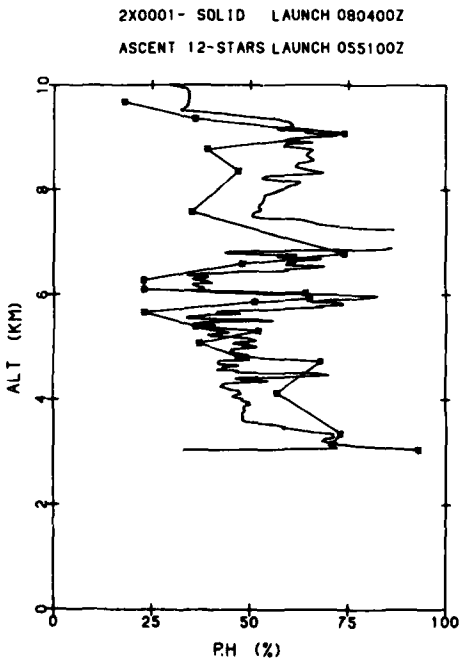

Figure 10. Comparison Between Relative Humidity Profile as Measured by Thermosonde 2X0001 and as Measured by Standard GMD Radiosonde, Ascent 12. Launched 20 Aug 1982, 0804Z

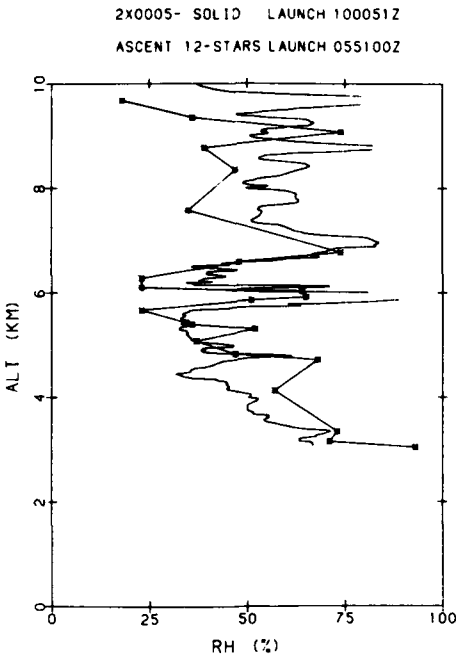

Figure 11. Comparison Between Relative Humidity Profile as Measured by Thermosonde 2X0005 and as Measured by Standard GMD Radiosonde, Ascent 12. Launched 20 Aug 1982, 1001Z

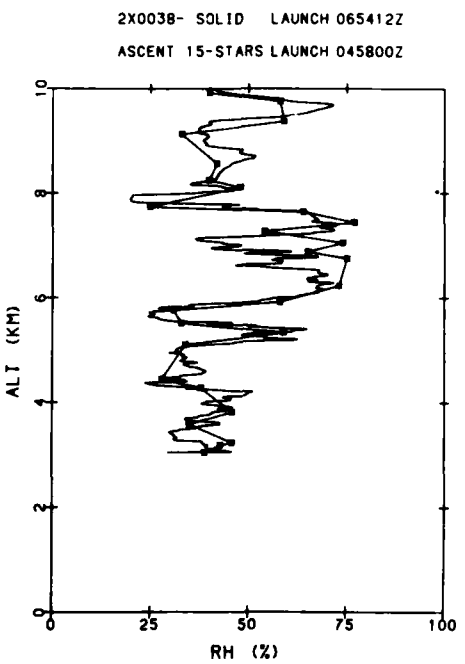

Figure 12. Comparison Between Relative Humidity Profile as Measured by Thermosonde 2X0038 and as Measured by Standard GMD Radiosonde, Ascent 15. Launched 21 Aug 1982, 0654Z

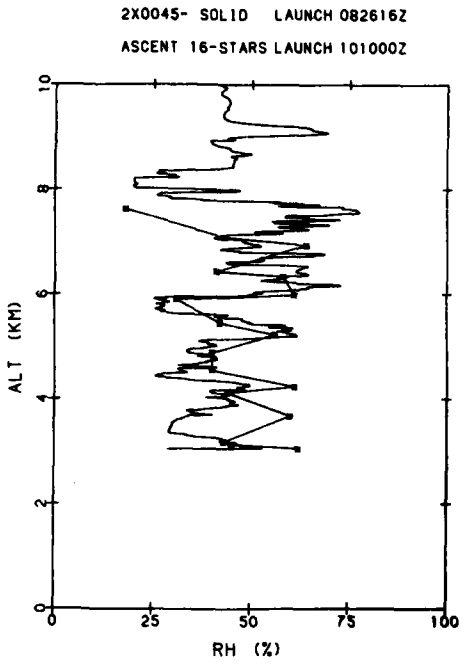

Figure 13. Comparison Between Relative Humidity Profile as Measured by Thermosonde 2X0045 and as Measured by Standard GMD Radiosonde, Ascent 16. Launched 21 Aug 1982, 0826Z

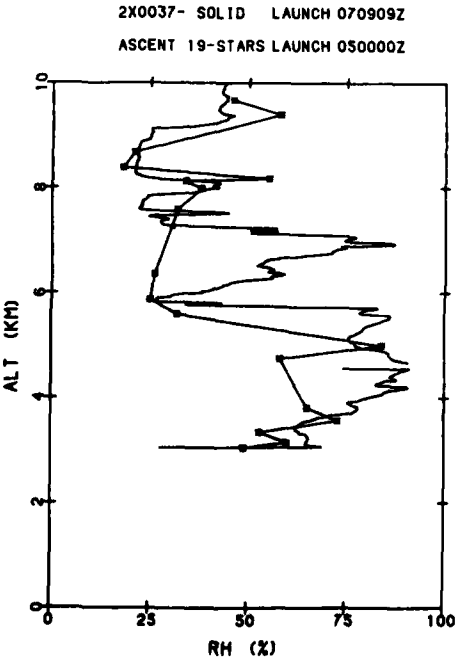

Figure 14. Comparison Between Relative Humidity Profile as Measured by Thermosonde 2X0037 and as Measured by Standard GMD Radiosonde, Ascent 19. Launched 22 Aug 1982, 0709Z

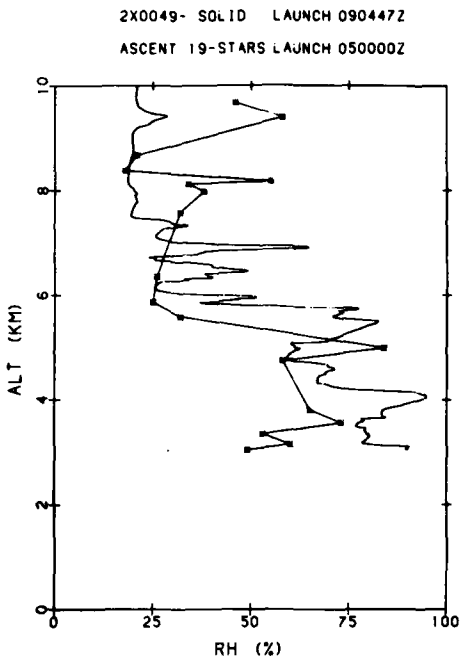

Figure 15. Comparison Between Relative Humidity Profile as Measured by Thermosonde 2X0049 and as Measured by Standard GMD Radiosonde, Ascent 19. Launched 22 Aug 1982, 0905Z

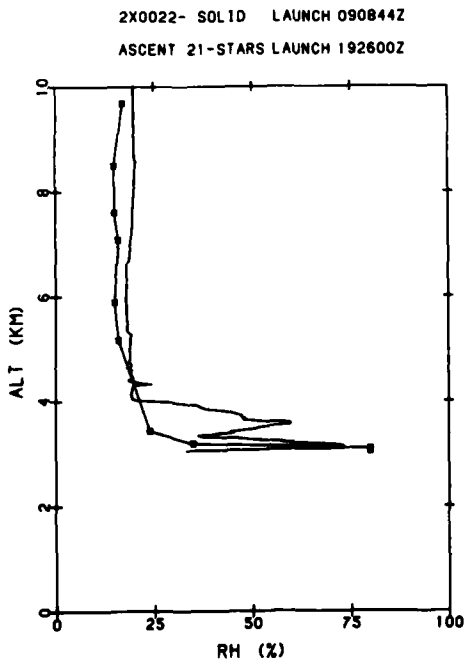

Figure 16. Comparison Between Relative Humidity Profile as Measured by Thermosonde 2X0022 and as Measured by Standard GMD Radiosonde, Ascent 21. Launched 22 Aug 1982, 0909Z

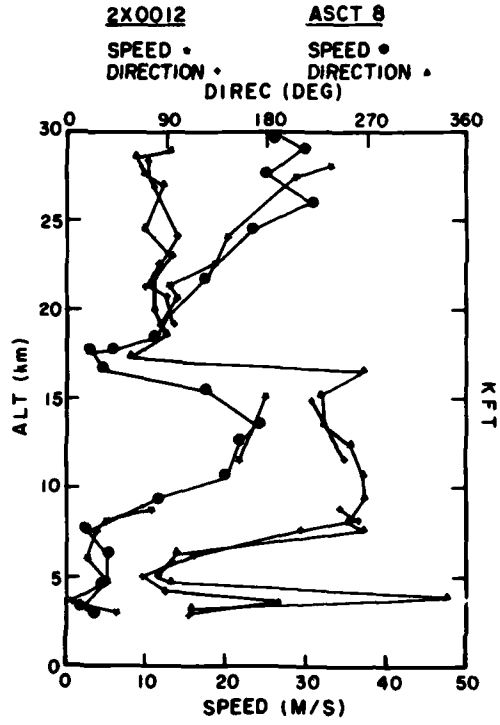

Figure 17. Comparison Between Wind Profile as Measured by Thermosonde 2X0012 and Standard GMD Radiosonde, Ascent 8. Launched 13 Aug 1982, 1041Z

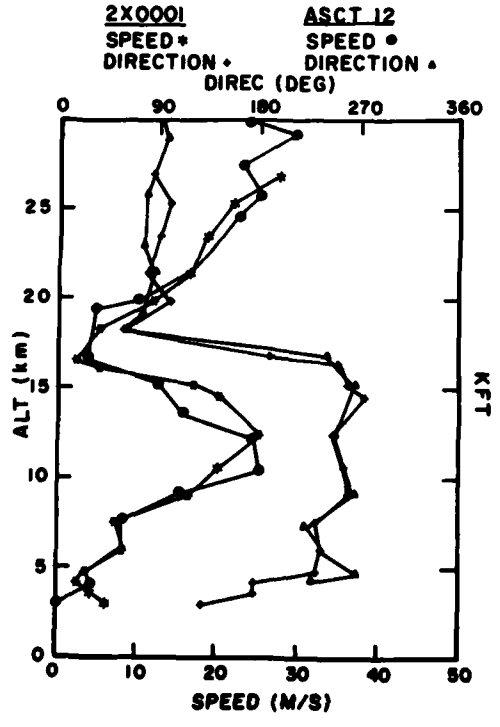

Figure 18. Comparison Between Wind Profile as Measured by Thermosonde 2X0001 and Standard GMD Radiosonde, Ascent 12. Launched 20 Aug 1982, 0804Z

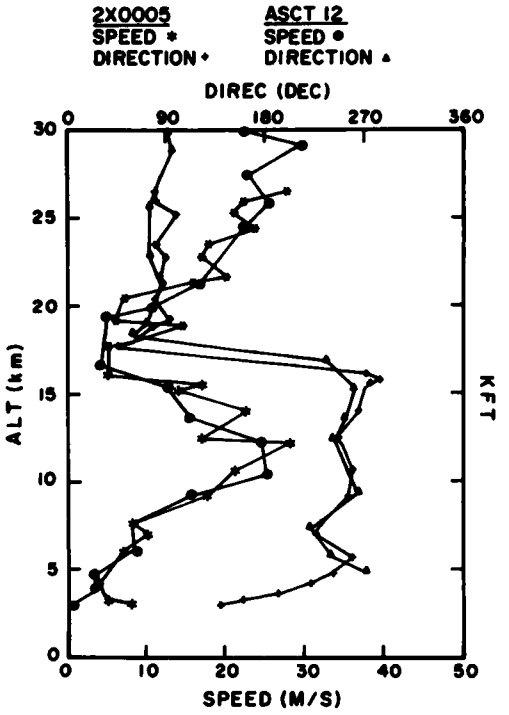

Figure 19. Comparison Between Wind Profile as Measured by Thermosonde 2X0005 and Standard GMD Radiosonde, Ascent 12. Launched 20 Aug 1982, 1001Z

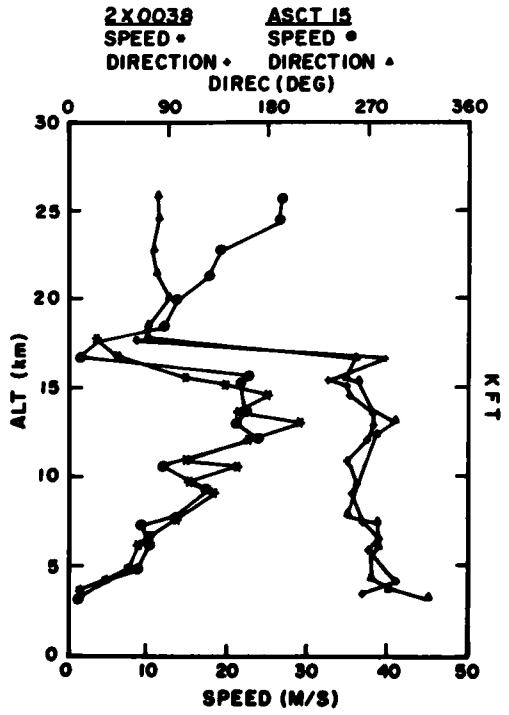

Figure 20. Comparison Between Wind Profile as Measured by Thermosonde 2X0038 and Standard GMD Radiosonde, Ascent 15. Launched 21 Aug 1982, 0654Z

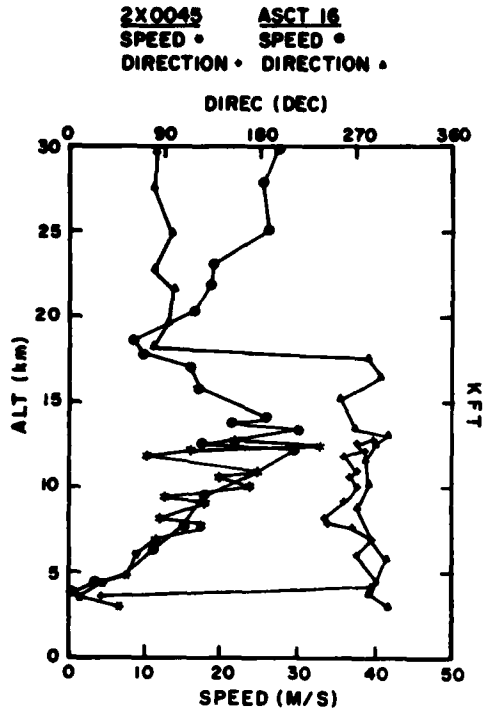

Figure 21. Comparison Between Wind Profile as Measured by Thermosonde 2X0045 and Standard GMD Radiosonde, Ascent 16. Launched 21 Aug 1982, 0826Z

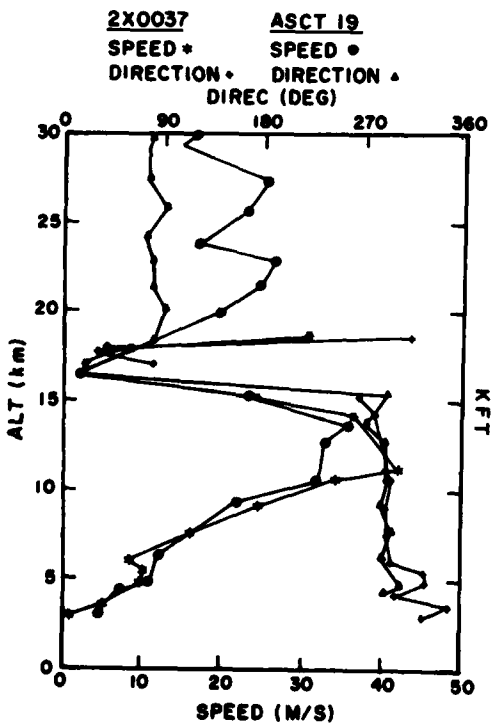

Figure 22. Comparison Between Wind Profile as Measured by Thermosonde 2X0037 and Standard GMD Radiosonde, Ascent 19. Launched 22 Aug 1982, 0709Z

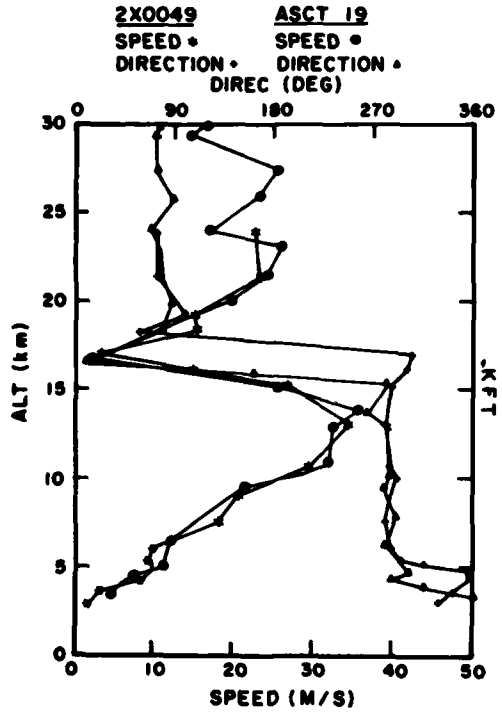

Figure 23. Comparison Between Wind Profile as Measured by Thermosonde 2X0049 and Standard GMD Radiosonde, Ascent 19. Launched 22 Aug 1982, 0905Z

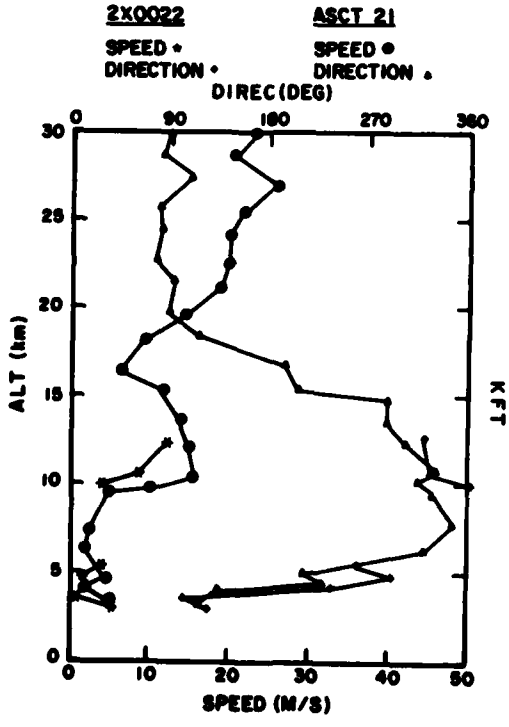

Figure 24. Comparison Between Wind Profile as Measured by Thermosonde 2X0022 and Standard GMD Radiosonde, Ascent 21. Launched 24 Aug 1982, 0909Z

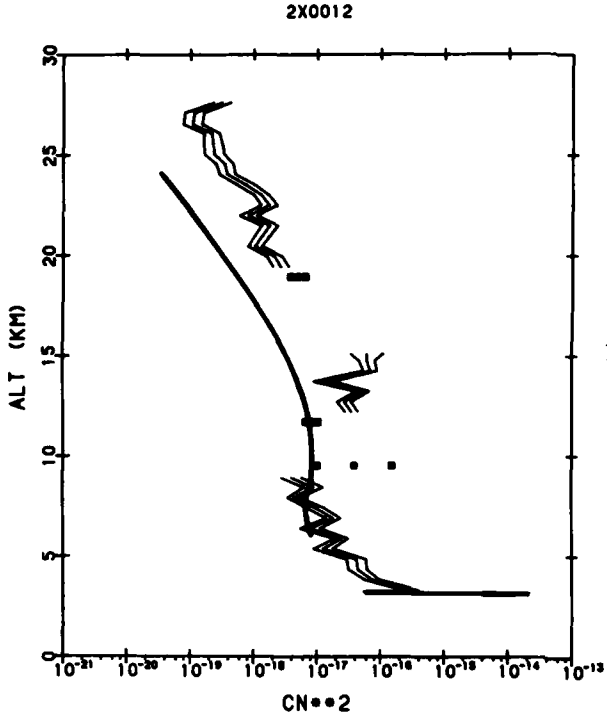

Figure 25. Comparison of 500-m Log-Averaged Thermosonde C_n^2 Profile (Mean Bracketed by Mean Multiplied by 1 Sigma and Mean Divided by 1 Sigma) and Hufnagel Model (Thick Line) for Thermosonde 2X0012 and Standard GMD Radiosonde, Ascent 8. Launched 13 Aug 1982, 1041Z

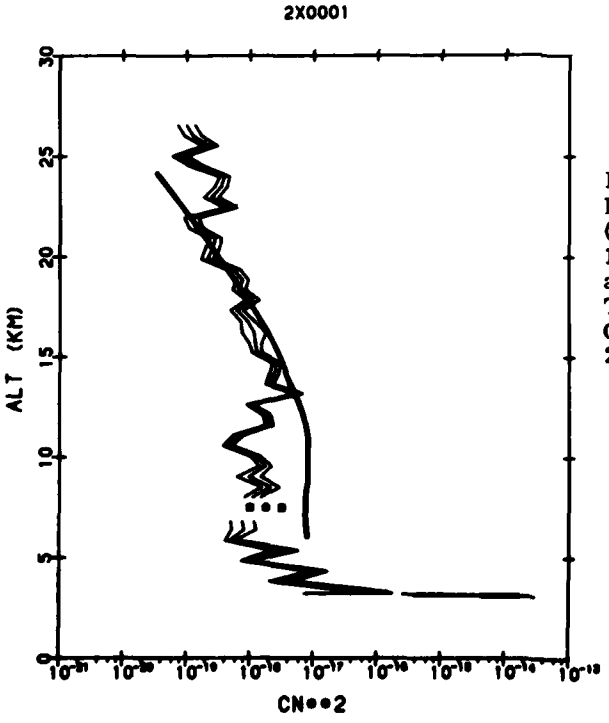

Figure 26. Comparison of 500-m Log-Averaged Thermosonde C_n^2 Profile (Mean Bracketed by Mean Multiplied by 1 Sigma and Mean Divided by 1 Sigma) and Hufnagel Model (Thick Line) for Thermosonde 2X0001 and Standard GMD Radiosonde, Ascent 12. Launched 20 Aug 1982, 0804Z

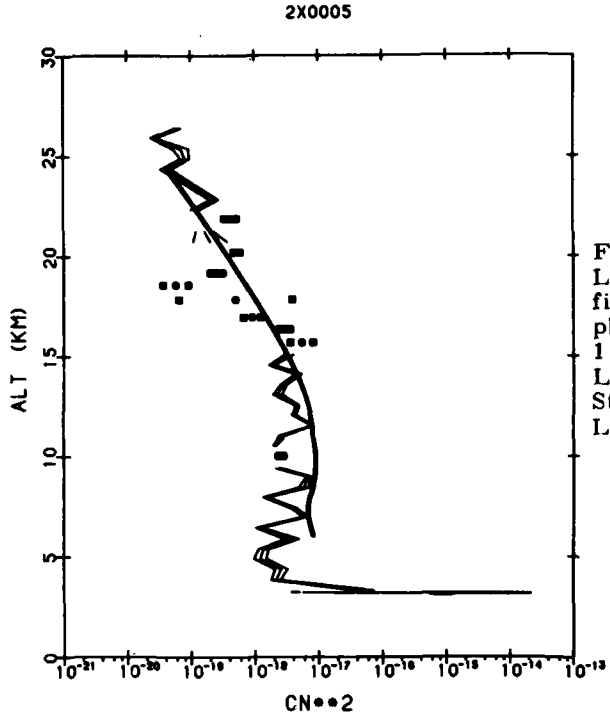

Figure 27. Comparison of 500-m Log-Averaged Thermosonde C_n^2 Profile (Mean Bracketed by Mean Multiplied by 1 Sigma and Mean Divided by 1 Sigma) and Hufnagel Model (Thick Line) for Thermosonde 2X0005 and Standard GMD Radiosonde, Ascent 12. Launched 20 Aug 1982, 1001Z

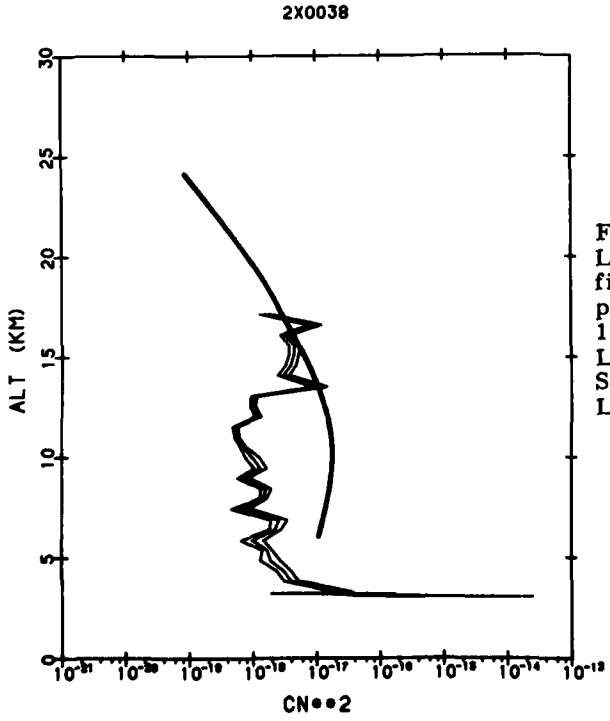

Figure 28. Comparison of 500-m Log-Averaged Thermosonde C_n^2 Profile (Mean Bracketed by Mean Multiplied by 1 Sigma and Mean Divided by 1 Sigma) and Hufnagel Model (Thick Line) for Thermosonde 2X0038 and Standard GMD Radiosonde, Ascent 12. Launched 21 Aug 1982, 0654Z

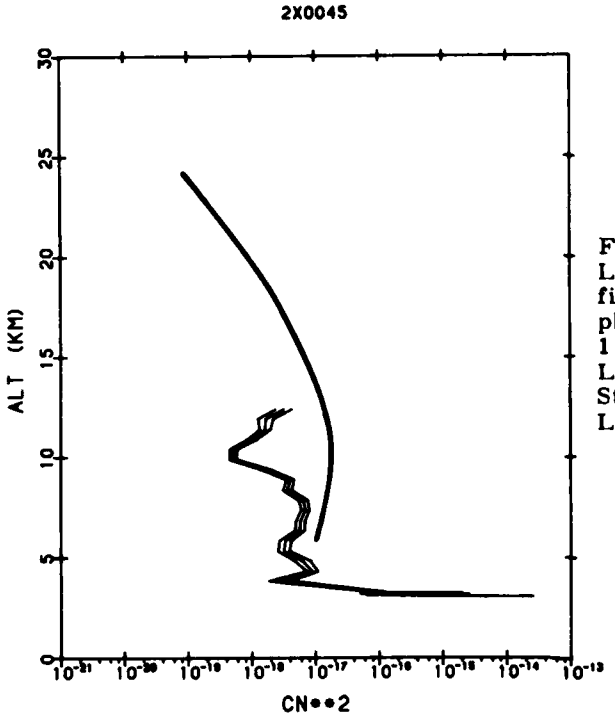

Figure 29. Comparison of 500-m Log-Averaged Thermosonde C_n^2 Profile (Mean Bracketed by Mean Multiplied by 1 Sigma and Mean Divided by 1 Sigma) and Hufnagel Model (Thick Line) for Thermosonde 2X0045 and Standard GMD Radiosonde, Ascent 16. Launched 21 Aug 1982, 0826Z

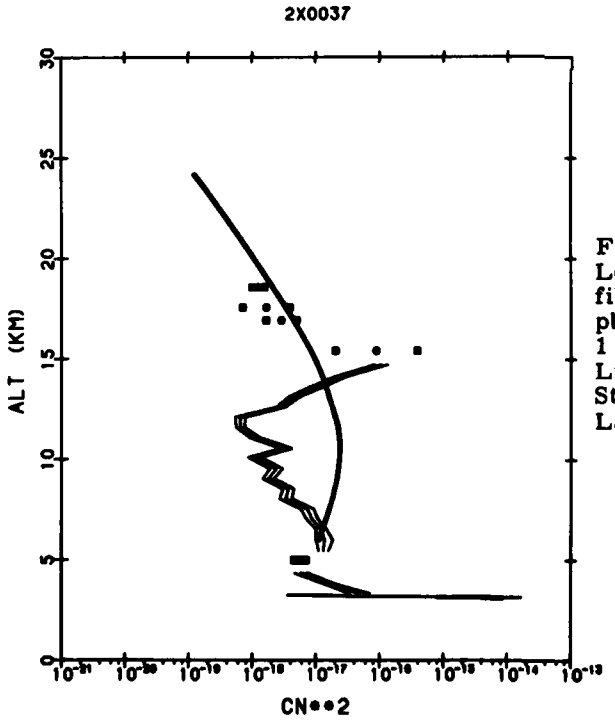

Figure 30. Comparison of 500-m Log-Averaged Thermosonde C_n^2 Profile (Mean Bracketed by Mean Multiplied by 1 Sigma and Mean Divided by 1 Sigma) and Hufnagel Model (Thick Line) for Thermosonde 2X0037 and Standard GMD Radiosonde, Ascent 19. Launched 22 Aug 1982, 0709Z

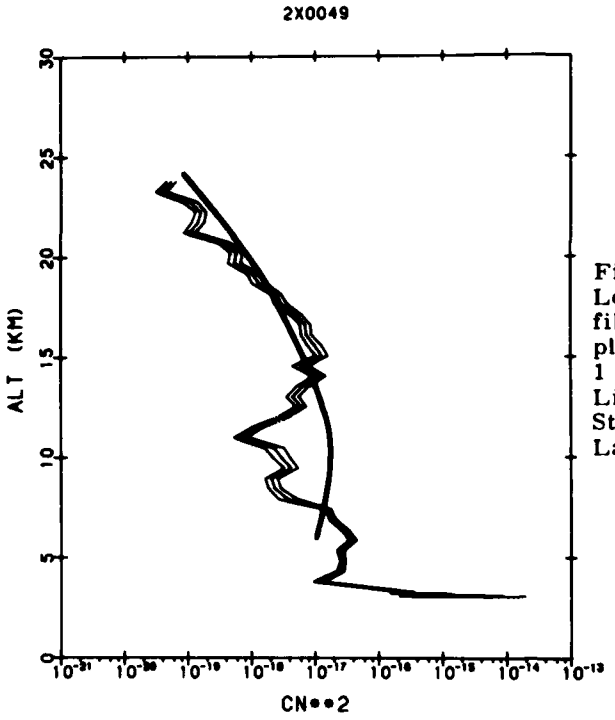

Figure 31. Comparison of 500-m Log-Averaged Thermosonde C_n^2 Profile (Mean Bracketed by Mean Multiplied by 1 Sigma and Mean Divided by 1 Sigma) and Hufnagel Model (Thick Line) for Thermosonde 2X0049 and Standard GMD Radiosonde, Ascent 19. Launched 22 Aug 1982, 0905Z

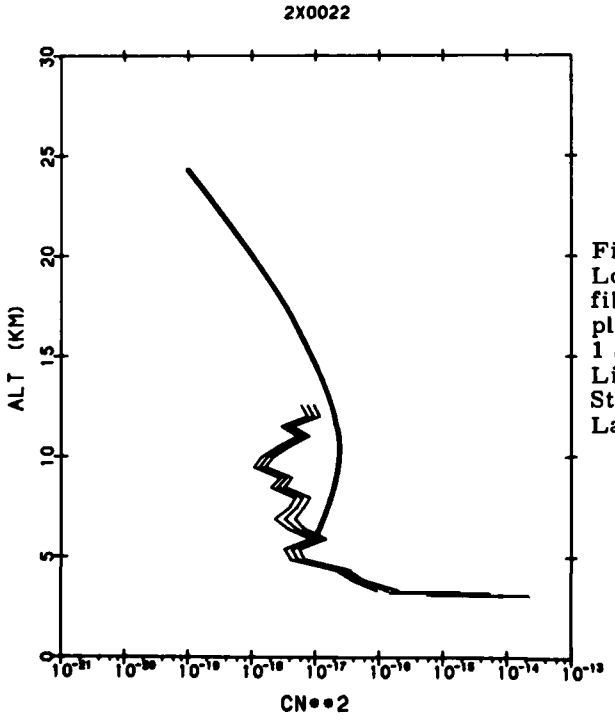

Figure 32. Comparison of 500-m Log-Averaged Thermosonde C_n^2 Profile (Mean Bracketed by Mean Multiplied by 1 Sigma and Mean Divided by 1 Sigma) and Hufnagel Model (Thick Line) for Thermosonde 2X0022 and Standard GMD Radiosonde, Ascent 21. Launched 24 Aug 1982, 0909Z

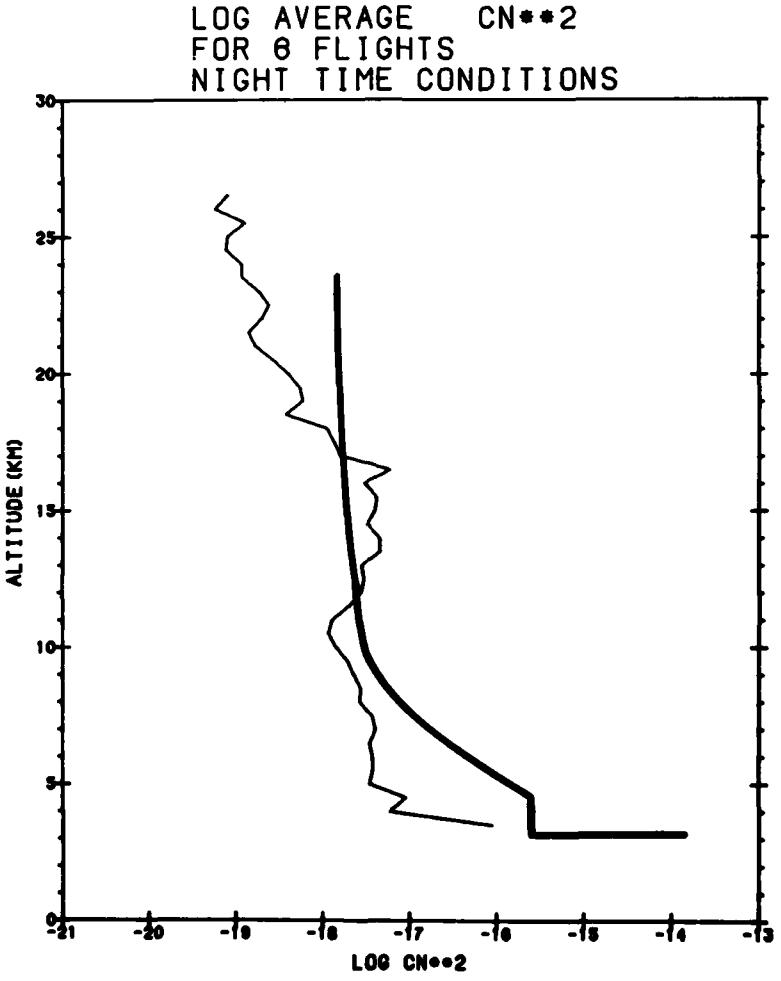

Figure 33. Comparison of Log-Averaged Thermosonde C_n^2 for Eight Flights and AMOS Model

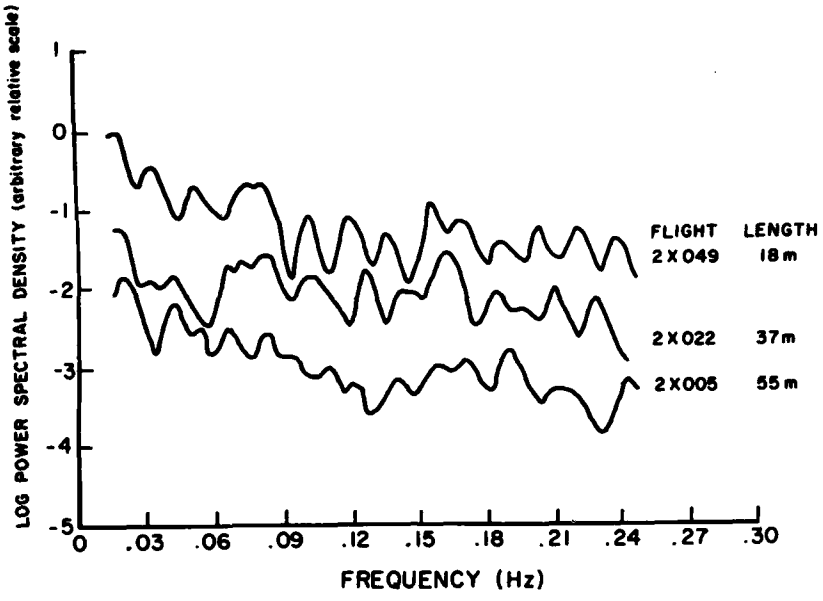

Figure 34. Comparison of PSDs for 18 m, 37 m, and 55 m Suspension Lengths, at Sample Altitude

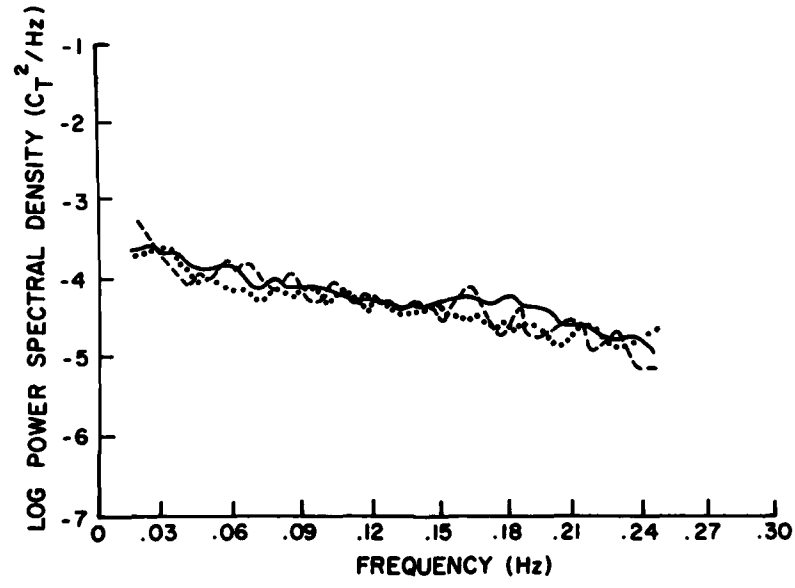

Figure 35. Comparison of PSDs for 18 m, 37 m, and 55 m Suspension Lengths, Averaged Over the Entire Altitude Region

References

1. Brown, J.H., Good, R.E., Bench, P.M., and Faucher, G.E. (1982) Sonde Experiments for Comparative Measurements of Optical Turbulence, AFGL-TR-82-0079, AD A118740.

2. Good, R.E., Brown, J.H., and Quesada, A.F. (1982) Measurements of high altitude resolution C_n^2 profiles and their importance on coherence lengths, SPIE Proc., 365:105-111.

3. Chapman, J.C. (1981) Groundbased infrared measurements using the AMOS/MOTIF facility, SPIE Proc., 280:186-193.

4. Hufnagel, R.E. (1974) Variations of Atmospheric Turbulence, The Infrared Handbook, USGPO, Washington, D.C., Chap. 6, pp. 1-56.

5. VanZandt, T.E., Gage, K.S., and Warnock, J.M. (1981) An improved model for the calculation of profiles of C_n^2 and ϵ in the free atmosphere from background profiles of wind, temperature and humidity, preprints 20th Conf. Radar Meteorol. Soc., Boston, Am. Meteorol. Soc., pp. 129-135.

6. Miller, M.G., and Zieske, P.L. (1979) Turbulence Environment Characterization, RADC-TR-79-131, AD A072379.

7. Miller, M.G., and Zieske, P.L. (1977) Measurement of the atmospheric correlation scale, J. Opt. Soc. Am., 67:1680-1685.

8. Good, R.E., Watkins, B.J., Quesada, A.F., Brown, J.H., and Loriot, G.B. (1982) Radar and optical measurements of C_n^2, Appl. Opt., 21 (No. 18):3373-3376.

END

FILMED

12-84

DTIC